

Comparative ontogeny, processing, and segmental distribution of the renal chloride channel, ClC-5

FRANÇOIS JOURET, TAKASHI IGARASHI, FRANÇOISE GOFFLOT, PATRICIA D. WILSON, FIONA E. KARET, RAJESH V. THAKKER, and OLIVIER DEVUYST

Division of Nephrology and Laboratory of Developmental Genetics, Université Catholique de Louvain, Brussels, Belgium; Department of Pediatrics, University of Tokyo, Tokyo, Japan; Division of Nephrology, Mount Sinai Medical School, New York, New York, USA; Department of Medical Genetics, Cambridge University, Cambridge, UK; and Nuffield Department of Medicine, University of Oxford, Oxford, UK

Comparative ontogeny, processing, and segmental distribution of the renal chloride channel, ClC-5.

Background. The renal chloride channel ClC-5, which is responsible for Dent's disease, is coexpressed with the vacuolar H⁺-ATPase in proximal tubules (PT) and α -type intercalated cells (IC) of the mature kidney. Neonatal cases of Dent's disease suggest that ClC-5 distribution must be acquired before birth. However, the ontogeny of ClC-5, and its processing and segmental distribution with respect to related proteins during nephrogenesis remain unknown.

Methods. Immunoblotting, real-time polymerase chain reaction (RT-PCR), immunostaining, and deglycosylation studies were used to investigate the expression, distribution, and maturation of ClC-5 during mouse and human nephrogenesis, in comparison with H⁺-ATPase, type II carbonic anhydrase (CAII), and aquaporin-1 (AQP1).

Results. An early induction (E13.5-E14.5) of ClC-5 was observed in mouse kidney, with persistence at high levels through late nephrogenesis. This pattern contrasted with the progressive expression of H⁺-ATPase and AQP1, and the postnatal upregulation of CAII. Immunostaining showed expression of ClC-5 in ureteric buds and, from E14.5, its location in developing PT. From E15.5, ClC-5 codistributed with H⁺-ATPase in PT cells and α -type IC. In the human kidney, ClC-5 was detected from 12 gestation weeks; its distribution was similar to that observed in mouse, except for a later detection in IC. Although mouse and human ClC-5 proteins are glycosylated, biochemical differences between fetal and adult proteins were observed in both species.

Conclusion. The segmental expression of ClC-5 and H⁺-ATPase is essentially achieved during early nephrogenesis, in parallel with the onset of glomerular filtration. These data give insight into PT and IC maturation, and explain early phenotypic variants of Dent's disease.

Key words: carbonic anhydrase, Dent's disease, endocytosis, H⁺-ATPase, intercalated cells, proximal tubule.

Received for publication February 18, 2003
and in revised form May 31, 2003
Accepted for publication August 11, 2003

© 2004 by the International Society of Nephrology

ClC-5 is an integral plasma membrane protein that belongs to the CLC family of voltage-gated chloride channels [1]. ClC-5 is encoded by the *CLCN5* gene, which is located on Xp11.22 and is predominantly expressed in the kidney [2]. Mutations in *CLCN5* are associated with Dent's disease, an X-linked renal tubular disorder characterized by low-molecular-weight proteinuria (LMWP) and renal Fanconi syndrome, associated with hypercalciuria, nephrocalcinosis, and nephrolithiasis [3, 4]. Studies in heterologous expression systems have shown that these mutations abolish or markedly reduce the outwardly rectifying chloride currents generated by ClC-5 [3].

The segmental expression of ClC-5 in the mature human and rat kidney includes the proximal tubule (PT), the thick ascending limb (TAL) of Henle's loop, and the α -type intercalated cells (IC) of the collecting duct (CD) [5–7]. The codistribution of ClC-5 with the vacuolar H⁺-ATPase in endosomes suggests that both proteins could interact to regulate endosomal acidification [5, 7] and apical targeting [8] in PT cells. The interaction between ClC-5 and H⁺-ATPase may also be important for the urinary acidification mediated by α -type IC [5–7]. These hypotheses are supported by the major defect in receptor-mediated endocytosis associated with PT dysfunction reported in ClC-5-deficient mice [9, 10], as well as by the alterations in polarity and expression of H⁺-ATPase observed in PT cells and IC from patients with Dent's disease [8].

The clinical manifestations of Dent's disease, including hematuria, proteinuria, mild polyuria, and nephrolithiasis may often occur during childhood, and LMWP is a consistent feature of the disease [4]. In particular, the early onset of some cases [11, 12], in which tubular proteinuria was discovered in the first month of life, suggests that segmental expression of ClC-5 in PT must be acquired before birth. Developmental studies in rats have shown that assembly of brush border components coincides with the onset of glomerular filtration [13], but the

status of other components of the endocytic pathway in PT cells, such as CIC-5 and H⁺-ATPase, is not known. Similarly, studies in rat kidney have shown that IC appear during late nephrogenesis and undergo postnatal maturation [14]. However, unlike rats, nephrogenesis in mouse and humans is essentially achieved at birth, and the pattern of appearance and differentiation of IC in these two species remains unclear.

In this study, we have investigated the renal ontogeny, processing, and distribution of CIC-5 during mouse and human nephrogenesis, in parallel with that of the vacuolar H⁺-ATPase, which provides the driving force for endosomal acidification in PT cells [15], type II carbonic anhydrase (CAII), which is essential for Na⁺ reabsorption and urinary acidification in PT cells [16], and the water channel aquaporin-1 (AQP1) as an ontogeny marker for PT cells [17]. These studies provide new insights into the maturation of PT and IC during nephrogenesis and help to understand the role of CIC-5 and the early phenotypic variants of Dent's disease.

METHODS

Human and mouse kidney samples

Human fetal kidneys from therapeutic abortion were procured by the International Institute for Advancement of Medicine (Philadelphia, PA, USA), the Anatomic Gift Foundation (Woodbine, GA, USA), and the Necker Hospital (Paris, France). Eighteen human fetal kidneys, ranging from 12 to 25 weeks of gestation (GW), were used for immunoblotting and immunostaining studies. For comparison and additional studies, we also used 3 newborn or infant human kidneys ranging in age from 4 months to 2 years. These normal kidneys were obtained directly at surgery and perfused with ice-cold neutral buffered salt solutions before processing for fixation and/or protein extraction [7, 17]. The use of these samples conformed to local ethical guidelines and were approved by the University of Louvain Ethical Review Board.

Mouse kidney samples were obtained from CD-1 mice (Iffa Credo, Brussels, Belgium). Pregnant mice were sacrificed by cervical dislocation, and embryos were dissected under a binocular to isolate kidneys. An average of 12 embryos from 4 different litters were collected every day from embryonic day 13.5 (E13.5) until day 5 after birth (newborn). Comparative studies were performed with 4 adult male kidneys. Kidney samples from wild-type versus CIC-5 knockout (KO) mice [10] and adult male Wistar rats were also used.

Antibodies

Affinity-purified polyclonal antibodies (SB499) directed against the N-terminus of human CIC-5 have been characterized previously [10]. Other antibodies in-

cluded a monoclonal antibody against the 31 kD E subunit (V1 domain) of the vacuolar H⁺-ATPase (a gift of Dr. S. Gluck, Washington University, St. Louis, MO, USA), a rabbit polyclonal antibody against the 116 kD a4 subunit (V0 domain) of the vacuolar H⁺-ATPase [18], a monoclonal antibody against β -actin (Sigma, St. Louis, MO, USA), a rabbit polyclonal antibody against AQP1 (Chemicon, Temecula, CA, USA), and sheep polyclonal antibodies against CAII (Serotec, Oxford, UK) and Tamm-Horsfall protein (Biodesign International, Kennebunk, ME, USA).

Immunoblot analyses and deglycosylation studies

Membrane extracts were prepared as previously described [7, 10]. Briefly, kidney samples were homogenized in ice-cold buffer (300 mmol/L sucrose and 25 mmol/L N-2-hydroxyethylpiperazine-N'-2-ethanesulfonic acid made to pH 7.0 with 1 mol/L tris (hydroxymethyl)amino-methane [Tris]) containing CompleteTM protease inhibitors (Roche, Vilvoorde, Belgium). The homogenate was centrifuged at 1000g for 15 minutes at 4°C, and the resulting supernatant was centrifuged at 100,000g for 120 minutes at 4°C. The pellet ("membrane" fraction) was suspended in ice-cold homogenization buffer before determination of protein concentration and storage at -80°C.

Deglycosylation studies were performed on human and mouse kidney extracts and control glycoproteins (Roche). The samples (15 μ g total protein) were incubated for 60 to 90 minutes at 37°C with 12 units of N-glycosidase F, as recommended by the manufacturer.

Immunoblotting was performed as previously described [7, 10]. After blocking, membranes were incubated overnight at 4°C with primary antibodies, washed, incubated for 1 hour at room temperature with appropriate peroxidase-labeled antibodies (Dako, Glostrup, Denmark), washed again, and visualized with enhanced chemiluminescence. Normalization for β -actin was obtained after stripping the blots and reprobing with the anti- β -actin antibody. Specificity of the immunoblot was determined by incubation with: (1) preimmune rabbit serum; (2) nonimmune rabbit or mouse immunoglobulin (Ig)G (Vector Laboratories, Burlingame, CA, USA) or control ascites fluid (Sigma); and (3) anti-CIC5 antibody preadsorbed with a 5-fold (w/w) excess of immunogenic peptide. Determination of the molecular mass was obtained by comparison with different precision standards (MBI Fermentas, Vilnius, Lithuania; Bio-Rad, Hercules, CA, USA). Densitometry analysis of the specific bands was performed with a Hewlett Packard Scanjet model IVC using the National Institutes of Health (NIH) Image V1.60 software, and optical densities normalized to β -actin density in the corresponding sample. All immunoblots were at least performed in duplicate.

RT-PCR and semiquantitative RT-PCR

Mouse kidney samples were homogenized in Trizol (Invitrogen, Merelbeke, Belgium) in order to extract total RNA. Total RNA samples (2.7 µg) were treated with DNase I (Invitrogen) and reverse-transcribed into cDNA using SuperScript II Rnase H Reverse Transcriptase (Invitrogen). The following primers were designed using Beacon Designer 2.0 (Premier Biosoft International, Palo Alto, CA, USA): CIC-5 (exon 6) sense 5' AAGTGG ACCCTTGTCATCAA 3' and antisense 5' ACAAG ATGTTCCACAGCAG 3', AQP1 (exons 1–2) sense 5' GCTGTCATGTATATCATCGCCAG 3' and antisense 5' AGGTCATTTCCGCCAAGTGAGT 3', GAPDH (exon 1) sense 5' TGCACCACCAACTGCTTAGC 3' and antisense 5' GGATGCAGGGATGATGTTCT 3'. The predicted lengths of the resulting PCR fragments were 115 bp (CIC-5), 107 bp (AQP1), and 176 bp (GAPDH). RT-PCR reactions were performed with 200 nmol/L of both sense and antisense primers in a final volume of 25 µL using 1 unit of Platinum Taq DNA polymerase, 2 mmol/L MgCl₂, 400 µmol/L dNTP. PCR conditions were 94°C for 5 minutes followed by 35 (CIC-5), 36 (AQP1), and 30 (GAPDH) cycles of 30 seconds at 95°C, 30 seconds at 61°C, and 1 minute at 72°C. The PCR products were size-fractionated on 1.5% agarose gel and then stained with ethidium bromide. Negative controls confirmed that the samples were not cross-contaminated (sterile water instead of RNA) or polluted by genomic DNA (not reverse-transcribed RNA samples). The expression of CIC-5 was also verified using another set of primers (exons 8–9), sense 5' TCC GCACAAACATTGCCTG 3' and antisense 5' AGGC AGCAGCCCCAACCAT 3' (predicted length of the fragment: 519 bp).

Real-time PCR analyses were performed in duplicate with 200 nmol/L of both sense and anti-sense primers in a final volume of 25 µL using 1 U of Platinum Taq DNA Polymerase, 2 mmol/L MgSO₄, 400 µmol/L dNTP, and SYBR Green I (Molecular Probe, Leiden, The Netherlands) diluted to 1/10⁵. PCR mixture contained 10 nmol/L fluorescein for initial well to well fluorescence normalization. PCR conditions were settled as incubation at 94°C for 3 minutes followed by 40 cycles of 30 seconds at 95°C, 30 seconds at 61°C, and 1 minute at 72°C. The melting temperature of PCR product was checked at the end of each PCR by recording SYBR green fluorescence increase upon slowly renaturing DNA. For each assay, standard curves were prepared by serial 4-fold dilutions of mouse adult kidney cDNA. The mRNA levels of CIC-5 and AQP1 were adjusted to GAPDH mRNA level at each stage, and relative changes in mRNA levels during ontogeny were determined by comparison to the adult mRNA level using the following formula: Ratio = (E_{target})^{ΔCt(Adult-Sample)} / (E_{GAPDH})^{ΔCt(Adult-Sample)} [19].

Immunostaining

Kidney samples were fixed in 4% paraformaldehyde (Boehringer Ingelheim, Heidelberg, Germany) in 0.1 mol/L phosphate buffer, pH 7.4, prior to embedding in paraffin as described [7, 10, 17]. Six µm sections were incubated for 30 minutes with 0.3% hydrogen peroxide to block endogenous peroxidase. For CIC-5 and H⁺-ATPase immunostaining, antigen retrieval was performed by incubating sections in 0.01 mol/L citrate buffer, pH 5.8, for 75 minutes, in a water bath heated at 97°C, before cooling down and rinsing. Following incubation with 10% normal serum for 20 minutes, sections were incubated for 45 minutes with the primary antibodies diluted in phosphate-buffered saline (PBS) containing 2% bovine serum albumin (BSA). After washing, sections were successively incubated with biotinylated secondary anti-immunoglobulin (Ig)G antibodies, avidin-biotin peroxidase, and aminoethylcarbazole (Vectastain Elite, Vector Laboratories). Sections were viewed under a Leica DMR coupled to a Leica DC300 digital camera (Leica, Heerbrugg, Switzerland). The specificity of immunostaining was tested by incubation: (1) in absence of primary antiserum; (2) with preimmune rabbit serum; (3) with non-immune rabbit serum or control rabbit or mouse IgG (Vector Laboratories); and (4) with the anti-CIC-5 antibody preadsorbed with the immunogenic peptide. The intensity of immunostaining was graded by an observer unaware of the embryonic stage and the antibody used, in comparison with the intensity observed in adult samples.

RESULTS

Comparative ontogeny of CIC-5 in the mouse kidney

CIC-5 was detected as a broad band at ~80 kD in the adult mouse kidney (Fig. 1A). The band was not detected in kidney extracts from *Cln5* KO mouse (left panel), or when the blot was incubated with anti-CIC-5 antibodies preadsorbed with the immunogenic peptide (right panel). The signal for CIC-5 observed in embryonic samples was different from the adult (right panel); it included two bands at ~90 kD and ~75 kD, respectively, separated by a smear of diffuse immunoreactive bands. With the exception of the upper band at ~90 kD, all the immunoreactive bands were abolished when using preadsorbed antibodies (right panel).

The expression of CIC-5 in the developing kidney was already detected at E13.5 (Fig. 1B). At this early stage, the immunoreactive pattern was characterized by the non-specific upper band at ~90 kD, and the diffuse specific bands including the ~75 kD band. The signal intensity for CIC-5 peaked early (E14.5), and remained quite stable to E16.5. From E16.5 to the newborn stage, the immunoreactivity pattern for CIC-5 showed a progressive decrease

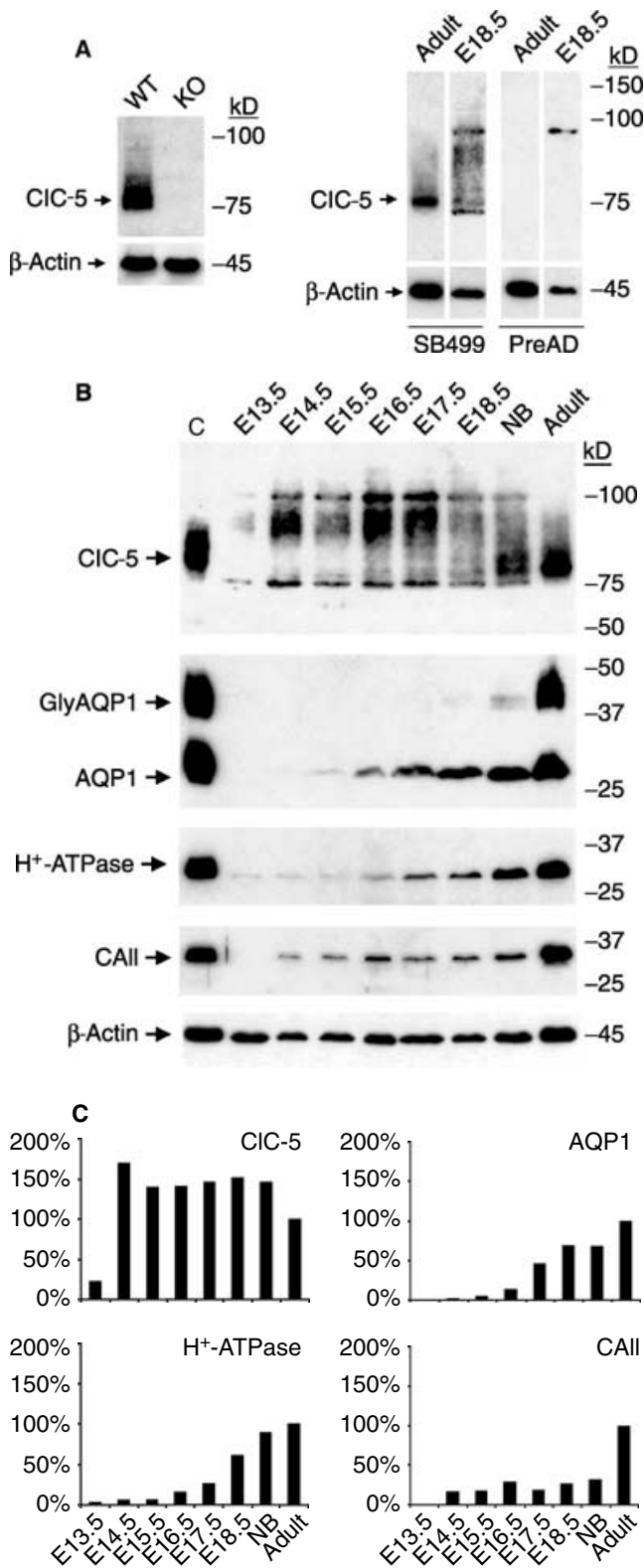


Fig. 1. Comparative ontogeny of CIC-5 in mouse kidney. (A) Characterization of the SB499 anti-CIC-5 antibodies. *Left:* Kidney extracts (30 μg/lane) from wild-type (WT) and knockout (KO) *Cicn5* mice were run on 7.5% PAGE and transferred to nitrocellulose. The blot was probed with SB499 anti-CIC-5 antibodies (1:1000). The diffuse band corresponding to CIC-5 at ~80 kD is absent in KO mice. The membranes

in the higher molecular mass isoforms and apparition of a more focused signal around 75 to 80 kD. Adult samples were characterized by concentrated immunoreactive bands around 80 kD, as described above.

The expression of AQP1 in the kidney is characterized by two isoforms—the core AQP1 (28 kD) and the glycosylated AQP1 (GlyAQP1, 35 to 50 kD). The core AQP1 was detected at E15.5 and it gradually increased during late ontogeny. The GlyAQP1 was detected only at E18.5 and in the newborn kidney, probably reflecting the increased amount of AQP1 [17]. The 31 kD band corresponding to the E1 subunit of the H⁺-ATPase was detected at low level from E13.5 and showed a gradual increase from E16.5 to birth. A progressive induction of the 116 kD a4 subunit of the H⁺-ATPase from E16.5, in parallel with the E subunit, was observed in developing mouse kidney (data not shown). The CAII band at 30 kD was detected at E14.5, remained stable during all ontogeny, and showed a dramatic increase postnatally (Fig. 1B). Densitometry analysis (Fig. 1C) confirmed the different expression patterns of CIC-5, which peaked at E14.5 (170% of adult level), remained high (140% to 150% of adult level) during ontogeny, and decreased after birth, AQP1 and H⁺-ATPase, which showed a gradual increase from E16.5, and CAII, with low expression levels (15% - 30% of adult level) during all ontogeny and a significant postnatal increase.

Quantification of CIC-5 mRNA expression in the developing mouse kidney

Semiquantitative (Fig. 2A) and real-time PCR analyses (Fig. 2B) confirmed the early induction of CIC-5 at

were stripped and reincubated with a monoclonal antibody against β-actin (1:10,000). *Right:* Adult and fetal (E18.5) mouse kidney extracts (20 μg/lane) were run on 7.5% PAGE and transferred to nitrocellulose. Identical strips were probed with control (SB499; 1:1000) or preadsorbed (PreAd; 1:1000) SB499 anti-CIC-5 antibodies. With the exception of the nonspecific upper band at ~90 kD detected in fetal samples, the distinct signal corresponding to CIC-5 in mature and developing kidney is abolished when incubation is performed with preadsorbed antibodies. Reprobing for β-actin was performed as above. (B) Representative immunoblots for CIC-5 in extracts from adult rat (positive control, C) and mouse at different stages—from E13.5 to E18.5, neonates (NB) and mouse at adult stages. Twenty μg of protein were loaded in each lane, and blots were probed with antibodies against CIC-5 (1:1000), AQP1 (1:20,000), H⁺-ATPase (1:100), CAII (1:1000), and after stripping, β-actin (1:10,000). CIC-5 is detected at E13.5, upregulated at E14.5, and then sustained during ontogeny. The immunoreactive pattern is also clearly different in the early (higher molecular mass bands) and late stages (focused immunoreactive bands around 75–80 kD) of maturation. The expression of AQP1 and H⁺-ATPase gradually increases from E16.5 and during late ontogeny, whereas CAII expression is characterized by post-natal upregulation. (C) Expression of CIC-5, AQP1, H⁺-ATPase, and CAII during mouse nephrogenesis: densitometry analyses of immunoblots. Values were obtained from duplicate blots and, after normalization over β-actin in each lane, compared with the adult kidney taken as the 100% reference. The early induction of CIC-5 contrasts with the progressive increase in AQP1 and H⁺-ATPase, and with the postnatal upregulation of CAII. The densitometry analyses of CIC-5 included all bands detected below the upper, nonspecific band at ~90 kD (see A).

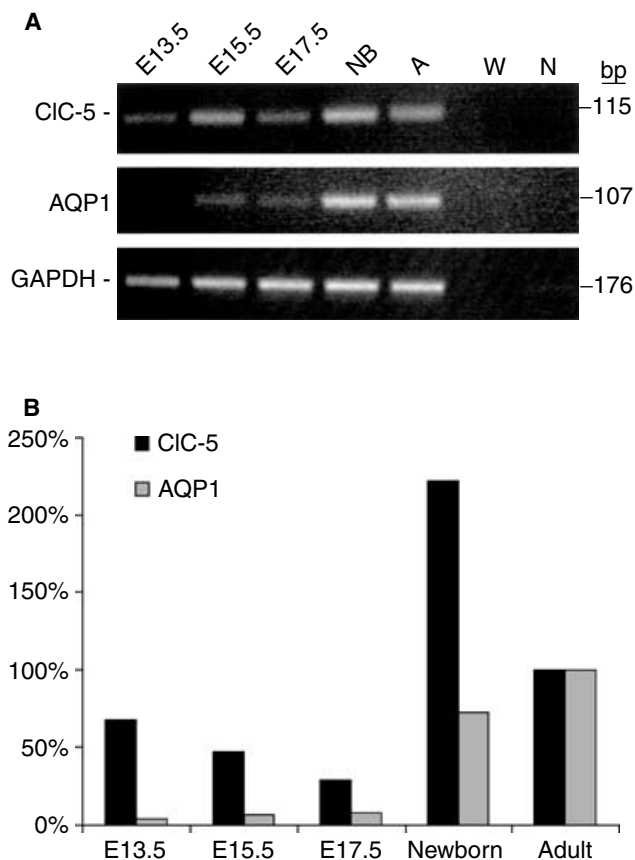


Fig. 2. Differential expression of CIC-5 and AQP1 in the developing mouse kidney: semi-quantitative and real-time PCR analysis. (A) Representative semiquantitative RT-PCR analysis of the expression of CIC-5, AQP1, and GAPDH during embryogenesis (E13.5, E15.5, E17.5) and in newborn (NB) and adult (A) mouse kidneys. Negative controls with water (W) and in absence of RT product (N) are shown. (B) Quantitative RT-PCR of CIC-5 and AQP1 mRNA expression during mouse nephrogenesis. The primers for CIC-5, AQP1, and GAPDH were similar to those used above. The CIC-5 and AQP1 mRNA levels were adjusted to GAPDH for each stage. The relative changes in expression during ontogeny were determined by comparison to the adult mRNA level taken as 100%. CIC-5 mRNA is significantly expressed at E13.5 (70% of the adult value), with a subsequent decrease until E17.5 (30%) and a major 2-fold upregulation at birth. This expression pattern contrasts with the low level of AQP1 at E13.5 (4% of the adult value) and its gradual increase from E15.5 (6%) to nearly reach the adult level at birth (73%).

E13.5, with a slight decrease of expression during late ontogeny, and a dramatic 2-fold increase in newborns. This expression pattern contrasted with that of the water channel AQP1, which showed a later induction at the end of nephrogenesis to nearly reach the adult level at birth.

Processing of CIC-5 during mouse nephrogenesis: Deglycosylation studies

Sequence analysis predicted that CIC-5 is a glycoprotein with N-glycans linked to Asn at position 408 [3]. Deglycosylation studies with N-glycosidase F were per-

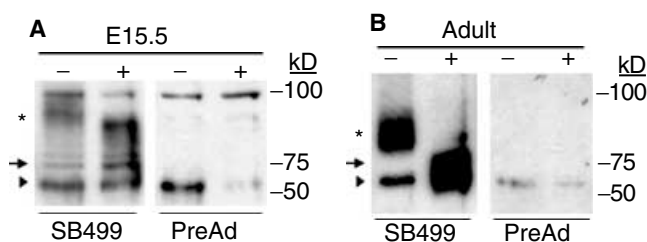


Fig. 3. Processing and glycosylation of CIC-5 in mouse kidney. The samples [(A) E15.5; (B) adult] were incubated with the reaction buffer containing (+) or not (-) N-glycosidase F, separated (7.5 μ g protein/lane) on 7.5% PAGE and probed with anti-CIC5 antibodies alone (SB499) or preadsorbed (PreAd) (both diluted 1:1000). Untreated embryonic samples (A) are characterized by diffuse immunoreactive CIC-5 bands (asterisk), located below the nonspecific 90 kD band, and by a 75 kD band (arrow). Incubation in the reaction buffer yielded a non-specific immunoreactive band at 60 kD (arrowhead) in all samples. Untreated adult samples (B) do not show the 75 kD band (arrow), but are characterized by a focused band at \sim 80 kD (asterisk), in addition to the nonspecific band at 60 kD (arrowhead). The shift of CIC-5-positive bands to a lower molecular weight after N-glycosidase F treatment indicates the existence of Asn-linked glycan chains in both embryonic and adult samples. It must be noted that embryonic samples differ from adult by the existence of a 75 kD, PGNase F-insensitive band, as well as by the higher molecular mass of the PGNase F-sensitive proteins in control and treated conditions.

formed in control glycoproteins and developing and adult mouse kidney samples (Fig. 3). Digestion of transferrin (65 to 60 kD), α 1-acid glycoprotein (45 to 22 kD), and ribonuclease B (17 to 15 kD) demonstrated the efficiency of deglycosylation (data not shown). Immunoblot analysis showed that untreated embryonic samples (Fig. 3A) are characterized by diffuse immunoreactive CIC-5 bands (asterisk) located below the nonspecific 90 kD band and a specific, core band at \sim 75 kD (arrow). The latter is above a nonspecific immunoreactive band at 60 kD (arrowhead), which results from incubation in reaction buffer. Untreated adult samples (Fig. 3B) showed the mature CIC-5 band at \sim 80 kD (asterisk) in addition to the nonspecific band at 60 kD (arrowhead), but not the 75 kD core band (arrow). Treatment with N-glycosidase F yielded a shift of the specific CIC-5-positive bands to a lower apparent molecular weight, indicating the existence of Asn-linked glycan chains in both embryonic and adult samples. To note, the molecular weight of the deglycosylated form of CIC-5 was slightly higher in developing than in mature kidney samples.

Ontogeny and glycosylation of CIC-5 in the human kidney

The broad immunoreactive band corresponding to CIC-5 was detected by immunoblotting in the developing human kidney at 12GW (Fig. 4A). The intensity of CIC-5 expression was sustained during all nephrogenesis, similar to that observed in the infant kidney. Treatment with N-glycosidase F induced a significant shift of

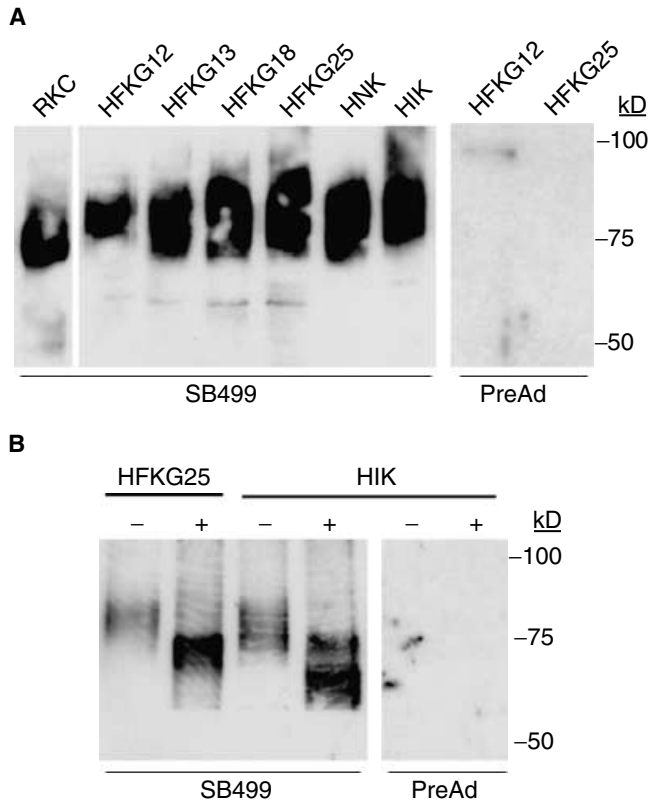


Fig. 4. Ontogeny and glycosylation of CIC-5 in the human kidney. (A) Representative immunoblot for CIC-5 in membrane extracts from rat kidney (positive control, RKC), human fetal kidney (HFK) at 12, 13, 18, and 25 GW, newborn (HMK) and infant (HIK) human kidney. Thirty μ g of protein were loaded in each lane, and the blot was probed with the anti-CIC-5 antibodies alone (SB499) or preadsorbed (PreAd) (both diluted 1:1000). The broad band corresponding to CIC-5 is detected at 12 GW, and its expression is sustained during nephrogenesis. The CIC-5 signal is abolished when incubation is performed with preadsorbed antibodies. Discrete bands below 60 kD are also detected with nonimmune IgG. (B) Deglycosylation with N-glycosidase F in human kidney samples (25 GW, HFK25; infant, HIK). The samples were incubated with the reaction buffer containing (+) or not (-) N-glycosidase F, separated (7.5 μ g protein/lane) on 7.5% PAGE and probed with anti-CIC-5 antibodies (SB499 lanes). The shift of CIC-5 bands to a lower molecular weight confirms the existence of Asn-linked glycan chains. As in mouse, the molecular mass of the PGNase F-sensitive CIC-5 proteins is higher in fetal than in postnatal samples. The pattern observed in HIK samples (more diffuse immunoreactive bands including lower mass isoforms) suggests that they may include residual embryonic isoforms. The signal is abolished when a similar blot is incubated with preadsorbed anti-CIC-5 antibodies (PreAd).

CIC-5-positive bands to a lower molecular weight (Fig. 4B), indicating the existence of Asn-linked glycan chains in developing and mature human kidney samples. As described in mouse, the molecular weight of the deglycosylated form of CIC-5 was higher in fetal than in postnatal samples.

Segmental distribution of CIC-5 during mouse nephrogenesis

CIC-5 was detected in the developing mouse kidney at E13.5 (Fig. 5A). The signal was located in branching

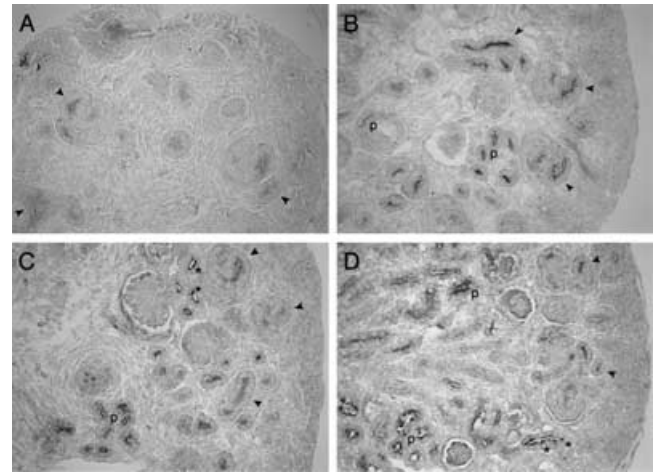


Fig. 5. Immunodetection of CIC-5 in the developing mouse kidney. (A) The staining for CIC-5 is first detected in the ureteric buds (arrowheads) located in the inner part of the primitive cortex at E13.5. (B) The staining intensity markedly increases at E14.5, with CIC-5 being located primarily in the ureteric buds (arrowheads) and developing PT (p). (C) CIC-5 staining at E15.5 and (D) E18.5 is observed in ureteric buds (arrowheads), and its intensity increases in developing PT (p); IC are detected from E15.5 (asterisks). Glomeruli, condensates, comma- and S-shaped bodies are negative (Original magnification A-D, \times 150).

ureteric buds within the inner part of the primitive cortex, whereas the undifferentiated metanephric cap tissue, the condensates, and the inner mesenchyme, were negative. Staining intensity for CIC-5 markedly increased at E14.5, by which dispersed primitive glomeruli were identified (Fig. 5B). The staining was stronger in the ureteric buds and also appeared in developing PT. Glomeruli, as well as comma- and S-shaped bodies, were all negative. From E15.5 (Fig. 5C) to E18.5 (Fig. 5D), CIC-5 staining persisted in ureteric buds, became more apparent in developing PT, and gradually appeared in the IC.

At higher magnification (Fig. 6), staining for CIC-5 within the primitive cortex of E14.5 kidneys was identified in the apical area of the tips of ureteric buds (Fig. 6A). A similar staining was observed within branching ureteric buds in the outer part of the primitive medulla (Fig. 6B), whereas an apical staining restricted to a subpopulation of ureteric buds cells was observed in the inner medulla (Fig. 6C). At E15.5, CIC-5 was identified in PT originating from recently formed glomeruli, and scattered CD cells (Fig. 6D and inset). The latter were also stained for apical H^+ -ATPase, indicating that they correspond to α -type IC (see below). At E16.5, CIC-5 showed a homogeneous, subapical staining in cells lining developing PT, and a strong apical staining in IC (Fig. 6E). To note, codistribution of CIC-5 (Fig. 6F) and Tamm-Horsfall protein (Fig. 6G) was observed in some juxtglomerular tubules at E16.5 and later. Distribution of CIC-5 in E18.5 kidneys included the apical area of PT cells and IC of the cortical CD (Fig. 6H), exactly like in newborn mouse (Fig. 6I). Codistribution of CIC-5 (Fig. 6J) and CAII (Fig. 6K)

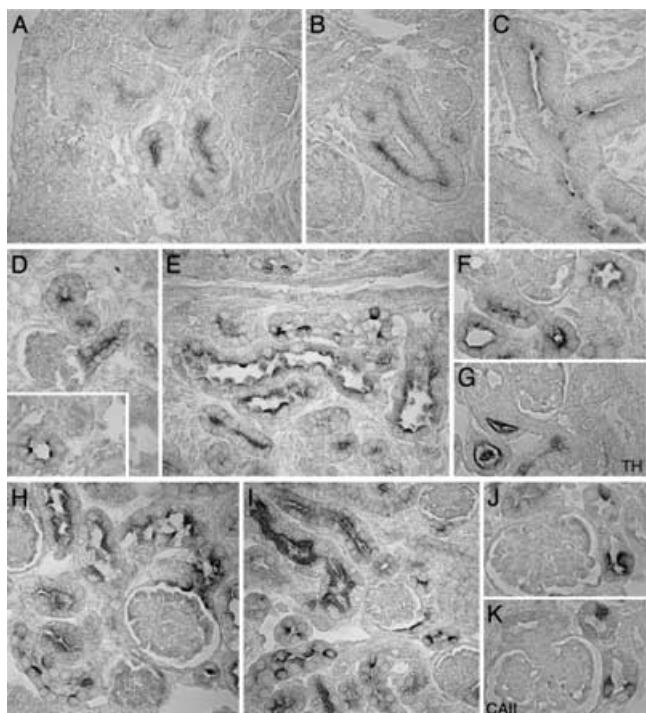


Fig. 6. Segmental distribution of CIC-5 during mouse nephrogenesis. (A, B, C, D, E, F, H, I, J) Immunostaining for CIC-5, (G) Tamm-Horsfall protein, and (K) CAII in the developing mouse kidney at (A–C) E14.5, (D) E15.5, (E–G) E16.5, (H) E18.5 (H), (I–K) and newborn kidney. At E14.5, staining for CIC-5 is restricted to the apical area of the (A, B) ureteric buds, and in a subpopulation of ureteric buds cells in the (C) inner medulla. At E15.5, CIC-5 is located in developing PT and scattered cells within developing CD in the (D) outer cortex. At (E) E16.5, linear apical CIC-5 staining is detected in PT cells, paralleled by a strong apical staining in IC within CD. Staining on serial sections from E16.5 kidneys shows codistribution of (F) CIC-5 and (G) Tamm-Horsfall protein in juxtglomerular tubules. The distribution of CIC-5 in PT and IC is exactly similar in (H) E18.5 and (I) newborn kidneys. Staining on serial sections shows the codistribution of (J) CIC-5 and (K) CAII in postnatal IC. (Original magnification: A–C, E, H, I, $\times 310$; D, F, G, J, K, $\times 410$).

was observed in postnatal IC. The specificity of CIC-5 staining was demonstrated with preadsorbed SB499 antibodies (data not shown). In comparison with CIC-5, CAII was first identified in IC at E15.5 and PT cells at E16.5, whereas AQP1 was detected in PT cells from E16.5 (data not shown). The distribution of CIC-5 and tubular markers during mouse nephrogenesis is summarized in Table 1.

Segmental distribution of H^+ -ATPase during mouse nephrogenesis

Staining for H^+ -ATPase was detected in the developing mouse kidney at E15.5 (Fig. 7A). The signal was located in the subapical area of developing PT in the inner cortex (Fig. 7E), whereas ureteric buds, glomeruli and undifferentiated structures were negative. Apical staining for H^+ -ATPase was also identified in scattered IC

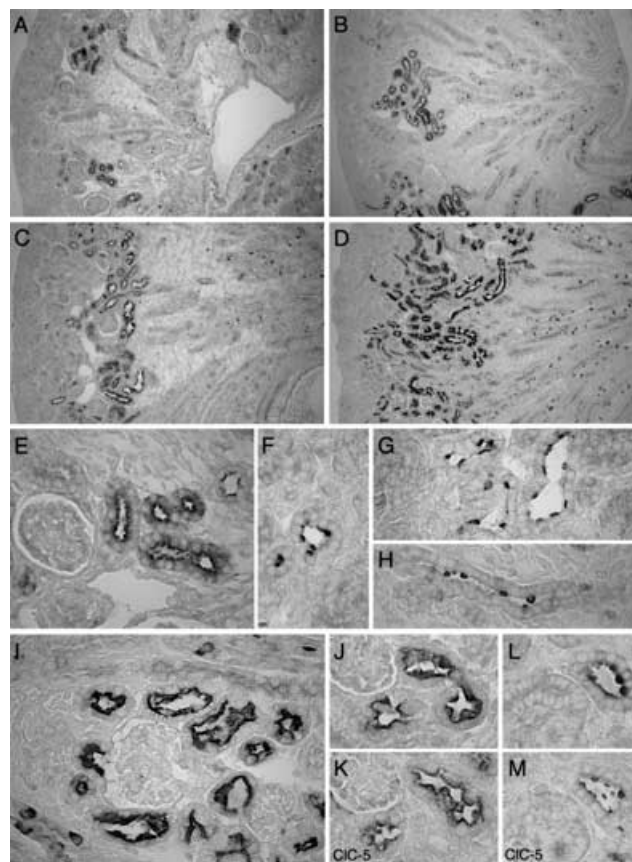


Fig. 7. Segmental distribution of H^+ -ATPase in the developing mouse kidney. (A–L) Immunostaining for H^+ -ATPase, and (K, M) CIC-5 in the developing mouse kidney at (A, E, F) E15.5 (B, G, H) E16.5 (C, J–M) E18.5, and (D, I) newborn kidney. (A) Staining for H^+ -ATPase is detected in developing tubules in the inner cortex at E15.5. (B) A progressive increase in staining is then observed at E16.5, (C) E18.5, and further in the (D) newborn, with a distribution that includes developing PT in the cortex and scattered IC within cortical and medullary CD. (E, F) At E15.5, H^+ -ATPase is located in the subapical area of developing (E) PT cells and scattered IC in (F) cortical CD. Numerous positive IC are also detected in the (G) cortical and (H) inner-medullary CD at E16.5. The H^+ -ATPase distribution during late ontogeny is similar to that observed in the (I) newborn kidney, including linear, subapical staining in PT cells and focal, apical staining in α -type IC. Staining on serial sections confirmed the colocalization of (K, M) CIC-5 with (J, L) H^+ -ATPase in (J, K) PT and (L, M) α -type IC. (Original magnification: A–D, $\times 80$; E, F, I–M: $\times 330$; G, H, $\times 385$).

(Fig. 7F). A significant increase in H^+ -ATPase expression was detected at E16.5 (Fig. 7B), with staining of developing PT and IC in the cortex and inner medulla (Fig. 7G and H). The IC in the medulla were characterized by apical protrusion into the lumen (Fig. 7H), unlike those observed in the cortex (Fig. 7G). The distribution of H^+ -ATPase at E18.5 (Fig. 7C) was similar to that observed in the newborn mouse kidney (Fig. 7D and I) and included PT cells (linear, subapical staining) and IC (punctuated, apical staining). H^+ -ATPase (Fig. 7J and L) and CIC-5 (Fig. 7K and M) colocalized in the developing PT and IC as early as E15.5 (see Table 1 for summary).

Table 1. Distribution of CIC-5, H⁺-ATPase, AQP1, and CAII in the developing mouse kidney: Summary

		E13.5	E14.5	E15.5	E16.5	E17.5	E18.5	Newborn
PT	CIC-5	(-)	(+)	(++)	(+++)	(+++)	(+++)	(+++)
	H ⁺ -ATPase	(-)	(-)	(+)	(++)	ND	(+++)	(+++)
	AQP1	(-)	(-)	(-)	(+)	(++)	(+++)	(+++)
	CA II	(-)	(-)	(-)	(+)	ND	(++)	(+++)
CCD	CIC-5	(+)UB tips	(++) UB tips	(++)UB tips Rare IC	(++) UB tips Numerous IC	(++) UB tips Numerous IC	Rare (++) UB tips Numerous IC	Rare (+) UB tips Numerous IC
	H ⁺ -ATPase	(-)	(-)	Rare IC	Numerous IC	ND	Numerous IC	Numerous IC
	AQP1	(-)	(-)	(-)	(-)	(-)	(-)	(-)
	CA II	(-)	(-)	Rare IC	Rare IC	ND	Numerous IC	Numerous IC
MCD	CIC-5	(-)	Rare UB cells	Rare IC	Numerous IC	Numerous IC	Numerous IC	Numerous IC
	H ⁺ -ATPase	(-)	(-)	Rare IC	Numerous IC	ND	Numerous IC	Numerous IC
	AQP1	(-)	(-)	(-)	(-)	(-)	(-)	(-)
	CA II	(-)	(-)	(-)	Rare IC	ND	Numerous IC	Numerous IC

Abbreviations are: PT, proximal tubule; CCD, cortical collecting duct; MCD, medullary collecting duct; UB, ureteric bud; IC, intercalated cells; ND, not done. Intensity of staining was graded as (-), absent; (+), weak; (++) , moderate; (+++) , strong.

Segmental distribution of CIC-5 and H⁺-ATPase in the developing human kidney

Diffuse staining for CIC-5 was identified in 13GW kidneys, located in developing PT from juxtamedullary nephrons (Fig. 8A and C). No specific staining was detected in condensates, comma and S-shaped bodies, and glomeruli. At 19 GW, a slightly more intense staining for CIC-5 was detected in maturing PT (Fig. 8B and D), whereas no specific staining was detected with preadsorbed SB499 antibodies (Fig. 8E). The distribution of CIC-5 in developing PT was confirmed in serial sections stained for AQP1; to note, the staining for AQP1 was more polarized than CIC-5 at that stage (Fig. 8F and G). In juxtamedullary nephrons, CIC-5 was also located in juxtglomerular tubule profiles that were positive for Tamm-Horsfall protein (Fig. 8H and I). In contrast with CAII (15GW) and H⁺-ATPase (19GW), CIC-5 could not be clearly identified in IC until the 24 GW (data not shown). Identification of CIC-5 staining in IC was ascertained postnatally by colocalization with CAII (Fig. 8J and K).

A faint signal for H⁺-ATPase (Fig. 9) was detected at 13 GW in the apical area of developing PT in the outer cortex, whereas glomeruli and ureteric buds were negative (Fig. 9A). From 15 GW to 24 GW (Fig. 9B), a progressive increase in H⁺-ATPase expression was detected in the subapical area of PT cells. Isolated cells positive for H⁺-ATPase (Fig. 9B) were also identified in the CD as early as 19 GW (inset of Fig. 9B). The reactivity for H⁺-ATPase after birth included a strong signal in the apical area of PT cells and IC of the CD (Fig. 9C).

DISCUSSION

Our studies show that CIC-5 undergoes a rapid induction at an early stage of mouse nephrogenesis, followed by a progressive maturation during late nephrogenesis. This

ontogeny pattern is distinct from the progressive increase of H⁺-ATPase and AQP1 expression, and the postnatal induction of CAII. Studies with PGNase F confirm the early N-linked glycosylation of CIC-5, and the progressive maturation of the core protein during nephrogenesis. The distribution of CIC-5 in PT and α -type IC, and its colocalization with H⁺-ATPase in these locations, are already achieved at E15.5 (see Table 1 for summary). In human nephrogenesis, CIC-5 is detected early during the second trimester, with a distribution that includes developing PT cells and later, IC.

Nephrogenesis in mouse and humans is characterized by a repetitive and reciprocal induction between the ureteric bud and the metanephric mesenchyme, resulting in the formation of a mature kidney before birth. In other species, such as rat or rabbit, nephrogenesis continues after birth ([20] for review). Glomerular filtration starts at E14 in mouse [21], and between the 9th and 12th GW in the human kidney [22]. The molecular events that take place in renal tubular cells following the onset of glomerular filtration remain partially unknown. The reabsorption of LMW proteins that are freely filtered is confined to PT cells, which are characterized by an intense endocytic activity followed by transport and degradation into the acidic vacuolar-lysosomal system [23]. Indirect evidence in rats [24] and humans [25] suggests that the PT endocytic activity is effective during nephrogenesis or immediately after birth. Furthermore, an increase of transporting membrane area and CA activity, as well as the upregulation of AQP1, has been documented in PT cells during nephrogenesis [17, 22, 26]. In contrast, the ontogeny and distribution of intracellular transporters such as CIC-5 and H⁺-ATPase during nephrogenesis have not been characterized to date. The issue is particularly relevant for PT maturation, since several lines of evidence suggest that CIC-5 interacts with the vacuolar H⁺-ATPase [8] and plays an essential role in the megalin receptor-mediated endocytic pathway [5, 7, 9, 10].

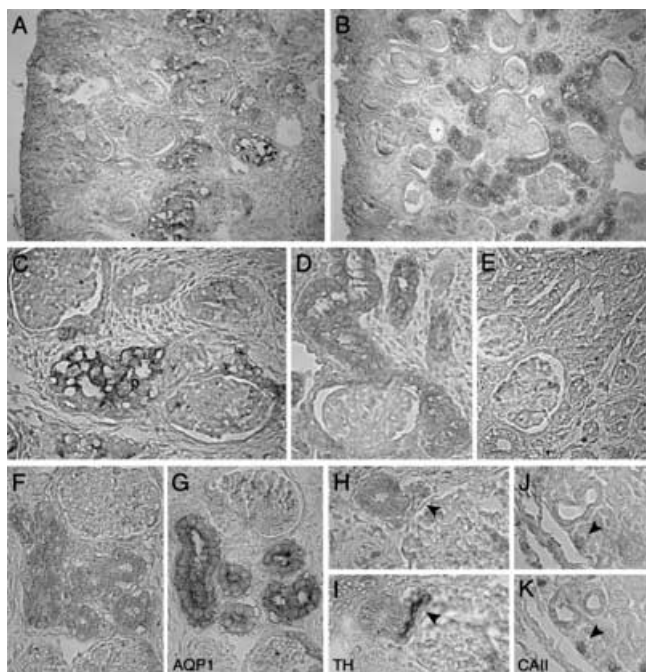


Fig. 8. Segmental distribution and co-localization of CIC-5 in the developing human kidney. Immunostaining for (A–F, H, J) CIC-5, (G) AQP1, (I) Tamm-Horsfall protein, and (K) CAII in the developing human kidney at (A, C) 13 GW, (E) 17 GW, (B, D) 19 GW, (F–I) 24 GW, and in a (J, K) 4-month infant kidney. Diffuse staining for CIC-5 is identified in developing PT (p) from juxtamedullary nephrons at 13GW, whereas (A, C) glomeruli are negative. A similar pattern is observed at 19 GW, with a slightly more intense staining for CIC-5 in maturing (B, D) PT. No specific staining is observed when using preadsorbed SB499 antibodies on similar sections (E). Staining on serial sections from 24 GW human kidneys demonstrated the colocalization of (F) CIC-5 and (G) AQP1 in PT. CIC-5 is also located in juxtamedullary tubule profiles (H, arrowheads) positive for (I) Tamm-Horsfall protein. Identification of CIC-5 staining in IC (J, arrowhead) is confirmed by colocalization with (K) CAII in serial sections from a 4-month-old kidney. (Original magnification: A, B, $\times 150$; C, J, K, $\times 300$; D, E, H, I, $\times 320$; F, G, $\times 280$).

Immunoblotting and RT-PCR analyses show that CIC-5 undergoes a rapid induction in the developing mouse kidney, followed by progressive maturation during late ontogeny and a marked induction just after birth (Figs. 1 and 2). Thus, the developmental pattern of CIC-5 expression in mouse clearly differs from that of another glycoprotein such as AQP1, or the co-expressed H^+ -ATPase. Studies with PGNase F not only confirmed the early N-glycosylation of CIC-5 [30] but also demonstrated biochemical differences between embryonic and adult CIC-5 proteins. These differences include the higher molecular mass of the PGNase F-sensitive proteins in embryonic versus adult samples, as well as the specific expression in mouse embryonic samples of a CIC-5 isoform (~ 75 kD) that is resistant to PGNase F treatment and that may correspond to the “core” CIC-5 protein (Fig. 3). By analogy with other members of the CLC family, the complex maturation of CIC-5 may result from alternative splicing [27, 28], post-translational modifications [29], or covalent binding to proteins that are expressed during

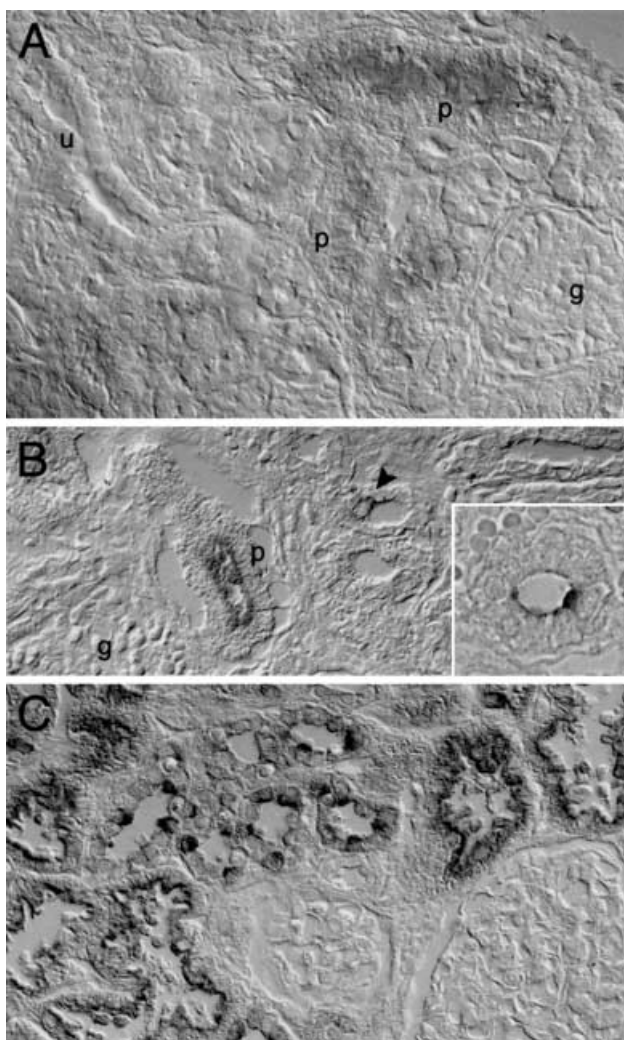


Fig. 9. Segmental distribution of H^+ -ATPase during human nephrogenesis. (A) At 13 GW, a faint signal for H^+ -ATPase is detected in the apical region of the developing PT (p) in the outer cortex. Glomeruli (g) and ureteric buds (u) are negative. (B) At 24 GW, H^+ -ATPase is located in PT cells (p) and IC (arrowhead). To note, the latter are already positive for H^+ -ATPase at 19 GW (inset). (C) Typical staining for H^+ -ATPase in a 2-year-old kidney includes PT cells and α -type IC within CD. (Original magnification: A, $\times 225$; B–D, $\times 425$).

nephrogenesis [20]. It is tempting to hypothesize that the transient expression of immature CIC-5 isoforms during ontogeny may correspond to the signal observed in ureteric buds, where there is no colocalization with H^+ -ATPase, whereas a progressive increase in mature CIC-5 isoforms may actually parallel the induction of H^+ -ATPase during late nephrogenesis. These results, and the postnatal regulation of CAII (Fig. 1C), confirm recent evidence showing that differentially regulated genes, including transporters, ion-motive ATPases, and enzymes, can be grouped in clusters that participate in different steps of kidney organogenesis [31].

As summarized in Table 1, the segmental expression of CIC-5 and H^+ -ATPase in PT cells is already detected at

E15.5 in mouse (Figs. 5 to 7), and essentially achieved during the second trimester of gestation in humans (Fig. 8). These results complete early observations that the apical expression of brush border components and the distribution of megalin to the apical clathrin-coated membrane domains and endosomes coincide with the onset of glomerular filtration in rats [13, 32]. The coexpression of CIC-5 and H⁺-ATPase in PT cells immediately after initiation of glomerular filtration could thus indicate the progressive maturation of renal tubular function and explain the decrease in the concentration of LMW proteins in the amniotic fluid during gestation [25]. These data also help to understand the pathophysiology of early phenotypic variants of Dent's disease, in which LMWP has been identified during the first weeks of life [11, 12].

In addition to PT cells, CIC-5 and H⁺-ATPase are codected from E15.5 in the apical area of isolated cells within the CD. The apical polarity of both markers allow to identify these cells as α -type IC, which, in the mature kidney, are primarily involved in urinary acidification. Studies in rat have shown that α -type IC simultaneously express H⁺-ATPase and CAII at the end of the gestation, mature and increase in number during the first weeks of life, and are then partially removed from the CD [14, 33]. Our results provide additional informations on IC maturation in mouse and human nephrogenesis. In mouse nephrogenesis, isolated cells of the medullary ureteric buds, positive for CIC-5, are detected as early as E14.5. IC positive for CIC-5, H⁺-ATPase, and CAII are observed in the cortical CD at E15.5. In human nephrogenesis, isolated cells positive for CAII are identified within ureteric buds and medullary CD at 15 GW, and rare, isolated cells positive for H⁺-ATPase are identified at 19 GW. In contrast, CIC-5 could not be identified in IC before 24 GW. The colocalization of CIC-5 with CAII and/or H⁺-ATPase in IC was only observed postnatally, confirming data obtained in mature kidney [5, 7]. These results suggest species differences in the maturation of IC [14, 33] and support the hypothesis that, in humans, the differentiation of IC occurs later than that of the principal cells of the CD [17]. Finally, CIC-5 is also located in tubules positive for Tamm-Horsfall protein, a marker of maturation of the TAL of Henle's loop [34]. The location of CIC-5 in maturing TAL confirms observations in mature human and rat kidney [6, 7]. It has been speculated that CIC-5 could play a role in the regulated Ca²⁺ reabsorption that occurs in TAL [35], providing a potential explanation for the hypercalciuria observed both in Dent's disease [4] and *CICN5* KO mice [10].

CONCLUSION

Our data demonstrate that the segmental distribution of CIC-5 and H⁺-ATPase is essentially achieved during early nephrogenesis in mouse and the second trimester

of gestation in humans. These data provide new insights in the maturation of renal tubules and help to understand the pathophysiology of early phenotypic variants of Dent's disease.

ACKNOWLEDGMENTS

We are grateful to P.J. Courtoy, N.Y. Loh, M.-Cl. Gubler, R. Rezzo-hazy, and F. Wu for helpful discussions and material, and to Ph. Camby, Y. Cnops, H. Debaix, and L. Wenderickx for excellent technical assistance. The *Cicn5* KO mice were kindly provided by W.B. Guggino (Dept. of Physiology, Johns Hopkins University Medical School, Baltimore, MD, USA). This work was supported by the Belgian agencies FNRS and FRSM, the Fondation Alphonse et Jean Forton, the Action de Recherches Concertées 00/05-260, and the Wellcome Trust (UK) and MRC (UK). F.J. is a Research Fellow of the FNRS.

Reprint requests to Olivier Devuyst, M.D., Ph.D., Division of Nephrology, Université catholique de Louvain, 10 Avenue Hippocrate, B-1200 Brussels, Belgium.
E-mail: devuyst@nefr.ucl.ac.be

REFERENCES

- JENTSCH TJ, STEIN V, WEINREICH F, ZDEBIK AA: Molecular structure and physiological function of chloride channels. *Physiol Rev* 82:503–568, 2002
- FISHER SE, BLACK GC, LLOYD SE, *et al*: Isolation and partial characterization of a chloride channel gene which is expressed in kidney and is a candidate for Dent's disease (an X-linked hereditary nephrolithiasis). *Hum Mol Genet* 3:2053–2059, 1994
- LLOYD SE, PEARCE SH, FISHER SE, *et al*: A common molecular basis for three inherited kidney stone diseases. *Nature* 379:445–449, 1996
- SCHNEIDERMAN SJ: X-linked hypercalciuric nephrolithiasis: Clinical syndromes and chloride channel mutations. *Kidney Int* 53:3–17, 1998
- GÜNTHER W, LÜCHOW A, CLUZEAUD F, *et al*: CIC-5, the chloride channel mutated in Dent's disease, co-localizes with the proton pump in endocytically active kidney cells. *Proc Natl Acad Sci USA* 95:8075–8080, 1998
- LUYCKX VA, GODA FO, MOUNT DB, *et al*: Intrarenal and subcellular localization of rat CIC-5. *Am J Physiol* 275:F761–F769, 1998
- DEVUYST O, CHRISTIE PT, COURTOY PJ, *et al*: Intra-renal and subcellular distribution of the human chloride channel, CLC-5, reveals a pathophysiological basis for Dent's disease. *Hum Mol Genet* 8:247–257, 1999
- MOULIN P, IGARASHI T, VAN DER SMISSEN P, *et al*: Altered polarity and expression of H⁺-ATPase without ultrastructural changes in kidneys of Dent's disease patients. *Kidney Int* 63:1285–1295, 2003
- PIWON N, GÜNTHER W, SCHWAKE M, *et al*: CIC-5 Cl⁻ channel disruption impairs endocytosis in a mouse model for Dent's disease. *Nature* 408:369–373, 2000
- WANG SS, DEVUYST O, COURTOY PJ, *et al*: Mice lacking renal chloride channel, CLC-5, are a model for Dent's disease, a nephrolithiasis disorder associated with defective receptor-mediated endocytosis. *Hum Mol Genet* 9:2937–2945, 2000
- NAKAZATO H, HATTORI S, FURUSE A, *et al*: Mutations in the *CICN5* gene in Japanese patients with familial idiopathic low molecular weight proteinuria. *Kidney Int* 52:895–900, 1997
- BOSIO M, BIANCHI ML, LLOYD SE, THAKKER RV: A familial syndrome due to Arg648Stop mutation in the X-linked renal chloride channel gene. *Pediatr Nephrol* 13:278–283, 1999
- BIEMESDERFER D, DEKAN G, ARONSON P, FAROUHAR MG: Assembly of distinctive coated pit and microvillar microdomains in the renal brush border. *Am J Physiol* 262:F55–F67, 1992
- KIM J, TISHER CC, MADSEN KM: Differentiation of intercalated cells in developing rat kidney: An immunohistochemical study. *Am J Physiol* 266:F977–F990, 1994
- MELLMAN I, FUCHS R, HELENIUS A: Acidification of the endocytic and exocytic pathways. *Annu Rev Biochem* 55:663–700, 1986

16. HAMM LL, ALPERN RJ: Cellular mechanisms of renal tubular acidification, in *The Kidney: Physiology and Pathophysiology*, edited by Seldin DW, Giebisch G, Philadelphia, Lippincott Williams & Wilkins, 2000, pp 1935–1979
17. DEVUYST O, BURROW CR, SMITH BL, et al: Expression of aquaporins-1 and -2 during nephrogenesis and in autosomal dominant polycystic kidney disease. *Am J Physiol* 271: F169–F183, 1996
18. SMITH AN, SKAUG J, CHOATE KA, et al: Mutations in ATP6N1B, encoding a new kidney vacuolar proton pump 116-kD subunit, cause recessive distal renal tubular acidosis with preserved hearing. *Nat Genet* 26:71–75, 2000
19. PFAFFI MW: A new mathematical model for relative quantification in real-time RT-PCR. *Nucleic Acids Research* 29:2004–2007, 2001
20. KUURE S, VUOLTEENAHO R, VAINIO S: Kidney morphogenesis: Cellular and molecular regulation. *Mech Develop* 92:31–45, 2000
21. LOUGHNA S, LANDELS E, WOOLF AS: Growth factor control of developing kidney endothelial cells. *Exp Nephrol* 4:112–118, 1996
22. BAUM M, QUIGLEY R: Postnatal renal development, in *The Kidney: Physiology and Pathophysiology*, edited by Seldin DW, Giebisch G, Philadelphia, Lippincott Williams & Wilkins, 2000, pp 703–725
23. CHRISTENSEN EI, NIELSEN S: Structural and functional features of protein handling in the kidney proximal tubule. *Semin Nephrol* 11:414–439, 1991
24. SMAOUI H, SCHAEVERBEKE M, MALLIE JP, SCHAEVERBEKE J: Transplacental effects of gentamicin on endocytosis in rat renal proximal tubule cells. *Pediatr Nephrol* 8:447–450, 1994
25. MUSSAP M, FANOS V, PICCOLI A, et al: Low molecular mass proteins and urinary enzymes in amniotic fluid of healthy pregnant women at progressive stages of gestation. *Clin Biochem* 29:51–56, 1996
26. LÖNNERHOLM G, WISTRAND PJ: Carbonic anhydrase in the human fetal kidney. *Pediatr Res* 17:390–397, 1983
27. BORSANI G, RUGARLI EI, TAGLIALATELA M, et al: Characterization of a human and murine gene (CLCN3) sharing similarities to voltage-gated chloride channels and to a yeast integral membrane protein. *Genomics* 27:131–145, 1995
28. LAMB F, GRAEFF RW, CLAYTONGH, et al: Ontogeny of CLCN3 chloride channel gene expression in human pulmonary epithelium. *Am J Respir Cell Mol Biol* 24:376–381, 2001
29. SHAILUBHAI K, SAXENA ES, BALAPURE AK, VIJAY IK: Developmental regulation of glucosidase I, an enzyme involved in the processing of asparagine-linked glycoproteins in rat mammary gland. *J Biol Chem* 265:9701–9706, 1990
30. ROTH J: Protein n-glycosylation along the secretory pathway: Relationship to organelle topography and function, protein quality control, and cell interactions. *Chem Rev* 102:285–303, 2002
31. STUART RO, BUSH KT, NIGAM SK: Changes in global gene expression patterns during development and maturation of the rat kidney. *Proc Natl Acad Sci USA* 98:5649–5654, 2001
32. SAHALI D, MULLIEZ N, CHATELET F, et al: Comparative immunochimistry and ontogeny of two closely related coated pit proteins. The 280-kd taget of teratogenic antibodies and the 330-kd taget of nephritogenic antibodies. *Am J Pathol* 142:1654–1667, 1993
33. NARBAITZ R, VANDORPE D, LEVINE DZ: Differentiation of renal intercalated cells in fetal and postnatal rats. *Anat Embryol (Berl)* 183:353–361, 1991
34. ZIMMERHACKL LB, ROSTASY K, WIEGELE G, et al: Tamm-Horsfall protein as a marker of tubular maturation. *Pediatr Nephrol* 10: 448–452, 1996
35. RICCARDI D, LEE WS, LEE K, et al: Localization of the extracellular Ca^{2+} -sensing receptor and PTH/PTHrH receptor in rat kidney. *Am J Physiol* 271:F951–F956, 1996